Developmental Biology 394 (2014) 110–121

Contents lists available at ScienceDirect

Developmental Biology

journal homepage: www.elsevier.com/locate/developmentalbiology

Polarized exocyst-mediated vesicle fusion directs intracellular lumenogenesis within the *C. elegans* excretory cell

Stephen T. Armenti [a,b], Emily Chan [a,b], Jeremy Nance [a,b,*]

[a] Helen L. and Martin S. Kimmel Center for Biology and Medicine at the Skirball Institute of Biomolecular Medicine, NYU School of Medicine, New York, NY 10016, USA
[b] Department of Cell Biology, NYU School of Medicine, New York, NY 10016, USA

ARTICLE INFO

Article history:
Received 26 March 2014
Received in revised form
8 July 2014
Accepted 26 July 2014
Available online 4 August 2014

Keywords:
Exocyst
PAR proteins
Lumenogenesis
Tubulogenesis
Vesicle trafficking
Osmoregulation

ABSTRACT

Lumenogenesis of small seamless tubes occurs through intracellular membrane growth and directed vesicle fusion events. Within the *Caenorhabditis elegans* excretory cell, which forms seamless intracellular tubes (canals) that mediate osmoregulation, lumens grow in length and diameter when vesicles fuse with the expanding lumenal surface. Here, we show that lumenal vesicle fusion depends on the small GTPase RAL-1, which localizes to vesicles and acts through the exocyst vesicle-tethering complex. Loss of either the exocyst or RAL-1 prevents excretory canal lumen extension. Within the excretory canal and other polarized cells, the exocyst co-localizes with the PAR polarity proteins PAR-3, PAR-6 and PKC-3. Using early embryonic cells to determine the functional relationships between the exocyst and PAR proteins, we show that RAL-1 recruits the exocyst to the membrane, while PAR proteins concentrate membrane-localized exocyst proteins to a polarized domain. These findings reveal that RAL-1 and the exocyst direct the polarized vesicle fusion events required for intracellular lumenogenesis of the excretory cell, suggesting mechanistic similarities in the formation of topologically distinct multicellular and intracellular lumens.

Introduction

Epithelial tubes enable the rapid distribution of liquids, gases, and circulating cells throughout the body. In larger tubes, multiple cells connected by junctions surround a common extracellular lumen (Andrew and Ewald, 2010; Iruela-Arispe and Davis, 2009). By contrast, small intracellular tubes, such as capillaries, can form within the cytoplasm of a single cell or cells connected in series. Intracellular tube formation requires the polarized targeting and fusion of cytoplasmic vesicles. For example, vertebrate vascular endothelial cells form a lumen when cytoplasmic vesicles accumulate in a central region of the cell and fuse with one another, or fuse with an invading apical membrane domain (Herwig et al., 2011; Davis and Camarillo, 1996). In terminal cells within the *Drosophila* trachea, as well as within the *Caenorhabditis elegans* excretory cell, lumenal membrane with apical character grows distally from the cell body and expands in length and diameter as a result of intracellular vesicle targeting and fusion (Kolotuev et al., 2013; Gervais and Casanova, 2010; Schottenfeld-Roames and Ghabrial, 2012; Khan et al., 2013). The molecular mechanisms responsible for the polarized membrane fusion events needed to create intracellular tubes are not well understood.

Polarization in many cells is mediated by the proteins PAR-3 (a multi-PDZ domain scaffolding protein), PAR-6 (a PDZ and CRIB domain scaffolding protein) and aPKC (an atypical protein kinase C) (Johnston and Ahringer, 2010; Nance and Zallen, 2011), which are collectively called PAR proteins. During polarization, upstream polarity cues induce PAR proteins to segregate asymmetrically within the cell, resulting in spatially restricted interactions between PAR proteins and their effectors. The role of PAR proteins in lumenogenesis has been investigated in canine epithelial (MDCK) cells grown in culture to form three-dimensional cysts (Bryant et al., 2010). MDCK cell cysts are similar to multicellular tubes, in that their formation requires the creation and expansion of extracellular space, rather than the intracellular membrane growth that is needed to form seamless tubes. MDCK cyst formation follows the transient recruitment of Par3 and vesicles to the site of future lumen formation at the cell surface, and knockdown of Par3 results in cysts containing multiple disorganized lumen-like structures. These findings suggest that Par3 and associated PAR proteins help to direct targeted vesicle fusion at the site of lumen formation. It is not known whether this mechanism is used to create multicellular tubes *in vivo*.

The eight-protein exocyst complex is also required for lumen formation in MDCK cell cysts (Bryant et al., 2010). In a wide variety

* Correspondence to: NYU School of Medicine, Skirball Institute of Biomolecular Medicine, 540 First Avenue, 4th floor, Lab. 17, New York, NY 10016, USA. Fax: +1 212 263 7760.
E-mail address: Jeremy.Nance@med.nyu.edu (J. Nance).

http://dx.doi.org/10.1016/j.ydbio.2014.07.019
0012-1606/

of organisms and cell types, the exocyst mediates vesicle tethering and subsequent fusion at specific sites on the cell membrane (Lipschutz et al., 2000; He and Guo, 2009; Liu and Guo, 2012). Six of the eight exocyst components are thought to associate with cytoplasmic exocytic vesicles (hereafter termed 'core exocyst' components), while Sec3 and Exo70 anchor the complex at the plasma membrane (Boyd, 2004). Small GTPases, including Ral, direct exocyst assembly and thereby promote vesicle tethering (Brymora et al., 2001; Sugihara et al., 2002; Moskalenko et al., 2002, 2003). Knockdown of exocyst function in MDCK cell cysts causes multiple disorganized lumens to form, similar to the phenotype of cysts lacking Par3. Moreover, Par3 and exocyst components show a mutually dependent localization during lumen formation (Bryant et al., 2010), and PAR proteins immunoprecipitate with exocyst components in multiple cell types (Lalli, 2009; Zuo et al., 2009, 2011; Rosse et al., 2009; Das et al., 2014). Recently, it was shown that the exocyst is also required for intracellular lumenogenesis within *Drosophila* terminal tracheal cells (Jones et al., 2014). These observations suggest that PAR proteins and the exocyst may cooperate to target vesicles to the cell surface during multicellular and intracellular lumenogenesis, although it remains unclear how the two protein complexes work together.

Here, using the *C. elegans* excretory cell as a model, we identify the exocyst as a downstream PAR effector responsible for driving vesicle fusion events that promote intracellular lumenogenesis. Required for maintaining osmotic balance (Nelson and Riddle, 1984), the excretory cell undergoes a rapid lumenal expansion during embryogenesis and the first larval stage (L1) to form an H-shaped seamless tube (canal) extending the length of the body (Fig. 1A) (Nelson et al., 1983). Lumen formation and expansion occur through the fusion of specialized vesicles, called canalicular vesicles, which surround the lumenal surface (Kolotuev et al., 2013). A cytoskeletal scaffold coats the cytoplasmic face of the lumen, preserving its shape and aiding in canalicular vesicle tethering or fusion (Göbel et al., 2004; Khan et al., 2013). We show that the exocyst concentrates at the lumenal scaffold and its activity is required for the fusion of canalicular vesicles that promotes lumenogenesis. Using early embryonic cells, we demonstrate upstream roles for RAL-1/Ral in recruiting the exocyst to the membrane and for PAR proteins in promoting exocyst membrane asymmetry. Our findings reveal an *in vivo* pathway that directs vesicle fusion events required for seamless intracellular tube formation, and suggest that topologically distinct intracellular and multicellular tubes can form using similar molecular mechanisms.

Results

The exocyst colocalizes with PAR proteins in the excretory cell and other polarized cell types

The expression and localization of the exocyst had not been described previously in *C. elegans*. There are *C. elegans* homologs of all eight exocyst components [*sec-3*, *sec-5*, *sec-6*, *sec-8*, *sec-10*, *sec-15*, *exoc-7* (*Exo70*) and *exoc-84* (*Exo84*)] as well as a single Ral homolog, *ral-1* (see Materials and methods). To determine whether the exocyst and RAL-1 are expressed during excretory canal morphogenesis, we created tagged fusion proteins for RAL-1 and the core exocyst components SEC-5, SEC-8, SEC-10 and SEC-15. Beginning at the onset of excretory canal formation and continuing through adult stages, tagged exocyst components and YFP-RAL-1 were present along the length of the excretory canal (Figs. 1A–C and S1A–C). Each tagged exocyst component and YFP-RAL-1 were also expressed maternally and therefore were present in cells of the early embryo. In particular, we noted a striking asymmetric localization of SEC-5-YFP, SEC-8-mCherry, mCherry-SEC-10 and SEC-15-YFP in polarized cells, including to the anterior membrane of one-cell embryos, the contact-free membrane of early embryonic cells, and the apical membrane of epithelial cells (Figs. 1E, F, H, and I, S1E–G; data not shown). PAR-3, PAR-6 and PKC-3/aPKC have similar asymmetries in these polarized cells (Nance and Zallen, 2011), which we confirmed by analyzing embryos co-expressing both SEC-8-mCherry and PAR-6-GFP (Figs. 1F, F′, I, and I′, S1G and G′). By contrast, YFP-RAL-1 displayed a more uniform plasma membrane enrichment (Fig. 1G and J).

To determine whether PAR proteins are also present in the excretory canal, we examined PAR-3 and PAR-6 reporters. Similar to SEC-8-mCherry, fluorescently tagged PAR-3 and PAR-6 were present along the length of the canal lumen (Figs. 1D, and S1D and D′), and we confirmed the excretory cell expression of endogenous PAR-6 and PKC-3 by immunostaining (Fig. S1H–I′′′). In summary, the exocyst and RAL-1 are found along the excretory canals together with PAR proteins, core exocyst components are asymmetric and co-localize with PAR proteins in polarized cells, and RAL-1 shows an overlapping but broader membrane localization.

ral-1 and the exocyst are essential for larval development and osmoregulation

To investigate the function of the exocyst, we examined mutations in *ral-1*, *sec-5*, and *sec-8* predicted to be strong loss-of-function or null alleles (see Materials and methods). *ral-1* (*tm5205*) lacks the start codon and first two exons of *ral-1*, which deletes a conserved region of the GTP-binding domain (van Dam and Robinson, 2006). *sec-8*(*ok2187*) deletes a central region of the *sec-8* locus, resulting in a frame shift and premature stop. *ral-1* (*tm5205*) and *sec-8*(*ok2187*) mutants displayed similar phenotypes, with most animals becoming sterile adults (Table S1). *sec-5* (*pk2358*) contains a nonsense mutation approximately halfway through the *sec-5* coding sequence (Frische et al., 2007). Most *sec-5* mutants were fertile, but ruptured at the vulva shortly after producing a few eggs, and all progeny died as embryos or L1 larvae. Phenotypes associated with each mutant allele were rescued by the respective tagged wild-type transgene (Table S1).

To determine how *ral-1*, *sec-5*, and *sec-8* mutant alleles affect the exocyst complex, we examined the localization of tagged exocyst components in each mutant, with the hypothesis that strong loss-of-function mutants would affect complex assembly. We focused on early embryonic cells because the exocyst complex shows a pronounced asymmetric localization in these cells, and because we previously developed tools to acutely remove gene function at this stage. To remove maternal contribution, we tagged *yfp-ral-1*, *sec-5-yfp*, and *sec-8-mCherry* transgenes with sequences encoding the PIE-1 protein ZF1 domain, which promotes rapid degradation of the tagged protein within early embryonic somatic cells (Reese et al., 2000; Nance et al., 2003). *zf1-yfp-ral-1*, *sec-5-zf1-yfp*, and *sec-8-zf1-mCherry* rescued the phenotypes of *ral-1*, *sec-5*, and *sec-8* mutants, respectively (Table S2). In each case, the ZF1-tagged protein degraded rapidly in early embryos, leaving cells lacking all functional sources of the gene product ('*MZ*' mutants, see Materials and methods). In *sec-5*(*MZ*) mutant embryos, exocyst marker mCherry-SEC-10 was lost from the membrane (Fig. S2A and A′). *ral-1*(*MZ*) mutants showed a similar loss in SEC-8-mCherry and mCherry-SEC-10 (Fig. S2A and A′ and data not shown), while exocyst markers were still present and asymmetric at the membrane in *sec-8*(*MZ*) early embryos (SEC-5-YFP, data not shown). Blocking degradation of ZF1-YFP-RAL-1 and SEC-5-ZF1-YFP by RNAi depletion of *zif-1*, which is required to destroy proteins tagged with the ZF1 domain (DeRenzo et al., 2003), rescued exocyst localization defects, indicating that these transgenes are functional at this stage (Fig. S2B, B′, D, and D′).

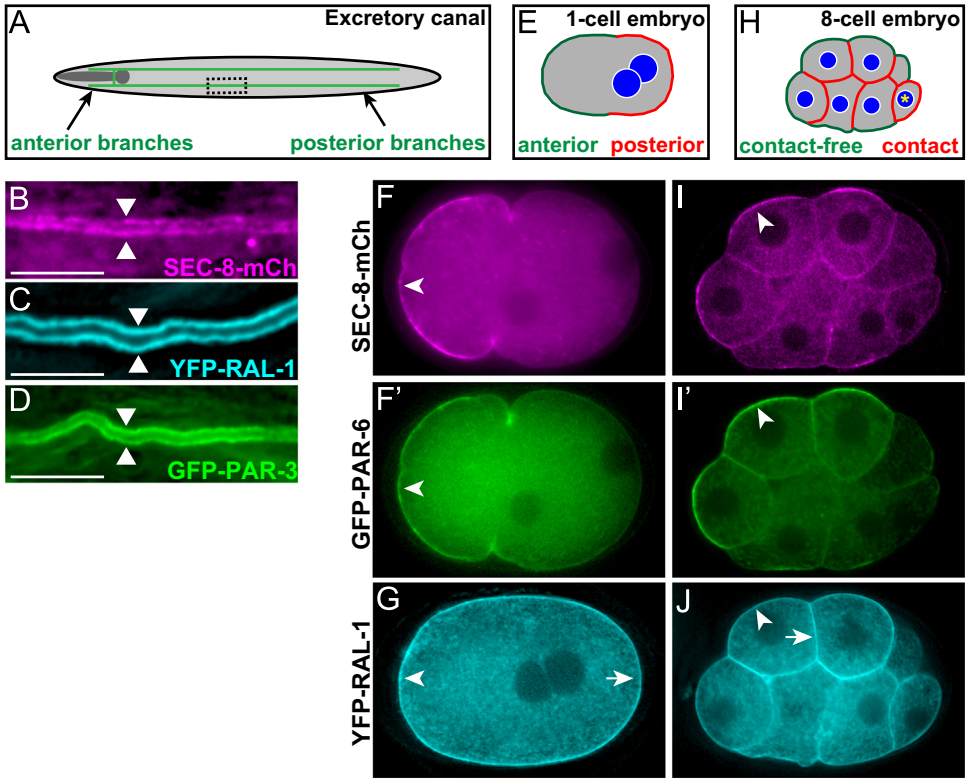

Fig. 1. RAL-1, exocyst and PAR protein expression in polarized cells. (A) Schematic of the excretory canal cell (green). The canal cell body and lateral branch are positioned adjacent the posterior pharynx (shaded dark gray). A representative region of posterior canal, depicted at higher magnification in (B–D), is indicated by dashed rectangle. (B–D) Lateral view of excretory canal segment in L4 larvae expressing the indicated fusion proteins; arrowheads point towards canal lumen. (E) Schematic of a polarized 1-cell embryo displaying distinct anterior and posterior membrane domains. (F and F′) 1-Cell embryo co-expressing SEC-8-mCherry (F) and PAR-6-GFP (F′), which are enriched at the anterior membrane (arrowheads). (G) 1-Cell embryo expressing YFP-RAL-1, which localizes uniformly to both anterior (arrowhead) and posterior (arrow) membranes. (H) Schematic of a polarized 8-cell embryo with distinct contacted and contact-free cell surfaces; the germline precursor cell (asterisk) is unpolarized. (I and I′) 8-Cell embryo co-expressing SEC-8-mCh (I) and PAR-6-GFP (I′), which are enriched at contact-free surfaces (arrowheads). (J) 8-Cell embryo expressing YFP-RAL-1, which localizes uniformly to contact-free (arrowhead) and contacted (arrow) surfaces. In this figure and all subsequent figures, embryos and larvae are oriented anterior to the left, and whole embryos are ~50 μm in length. Scale bars in (B–D) are 10 μm.

Therefore, while the alleles *ral-1*(*tm5205*) and *sec-5*(*pk2358*) prevent exocyst membrane assembly, *sec-8*(*ok2187*) affects exocyst function distinctly.

In contrast to zygotic mutants, *ral-1*(*MZ*), *sec-5*(*MZ*) and *sec-8* (*MZ*) mutants arrested primarily at the L1 larval stage (Table S3), with a small percentage of mutants arresting during embryogenesis. *sec-5*(*MZ*) mutants obtained as embryos and larvae laid by *sec-5* homozygous mothers displayed similar phenotypes and died at the same stage as those generated by ZF1-tagging ($n=26$). Therefore, despite the polarized localization pattern of the exocyst in early embryos, loss of exocyst function at this stage does not cause major developmental defects in most embryos. *ral-1*(*MZ*), *sec-5*(*MZ*) and *sec-8*(*MZ*) mutants that hatched were extremely sensitive to changes in osmolarity, accumulating fluid-filled cavities and dying quickly when placed in water (Fig. 2A and B). This phenotype is characteristic of mutants with defects in excretory cell function (Nelson and Riddle, 1984; Buechner et al., 1999), suggesting a role for RAL-1 and the exocyst in formation or function of the excretory cell.

The exocyst is required for excretory cell canal lumenogenesis

We analyzed excretory cell morphology in *ral-1*(*MZ*) and *sec-5* (*MZ*) mutants by expressing cytoplasmic GFP from the excretory cell-specific *pgp-12* promoter (Zhao et al., 2005). In newly hatched wild-type L1 larvae, short lumenized anterior canals extended toward the nose, and longer lumenized posterior canals extended approximately halfway to the posterior (Fig. 2C) (Buechner et al., 1999; Kolotuev et al., 2013). A thin non-lumenized cytoplasmic projection extended just beyond the lumen as the canal elongated, as described previously (Kolotuev et al., 2013), and by the end of the L1 stage, the lumen and cytoplasm both extended the length of the body. Previously described (Kolotuev et al., 2013) periodic regions of cytoplasmic swelling were present along the canal length (Fig. 2C, asterisks). In contrast, canals in *ral-1*(*MZ*) ($n=45$) and *sec-5*(*MZ*) ($n=43$) L1 larvae were disorganized and failed to properly elongate, containing much shorter and more irregular posterior canal branches (Figs. 2D and E, and S3). In a small fraction of *ral-1*(*MZ*) (3/45) and *sec-5*(*MZ*) (11/43) mutant L1 larvae, we failed to detect even a rudimentary lumen. Mutant L1 worms left on agar plates for several days often developed posterior extensions that could reach the end of the body, but that failed to lumenize and contained vacuoles (Fig. S3 and data not shown). These findings indicate that *ral-1* and *sec-5* are required for proper lumenogenesis within the canal, and are not essential for outgrowth of the non-lumenized canal basal extension. The presence of a rudimentary, disorganized and shortened lumen in mutants suggests either that canal lumen initiation occurs through an independent mechanism, or that *ral-1*(*MZ*) and *sec-5*(*MZ*) mutants retain sufficient function to allow for canal lumen initiation but not extension.

To assess exocyst function in less disorganized canals, we examined *ral-1* and *sec-5* zygotic mutants. In L4 larvae, the lumenized posterior canals of *ral-1* and *sec-5* mutants terminated prematurely, before reaching the tail (Figs. 2F–H, and S4B). Lumens in both mutants typically ended with a bulge containing

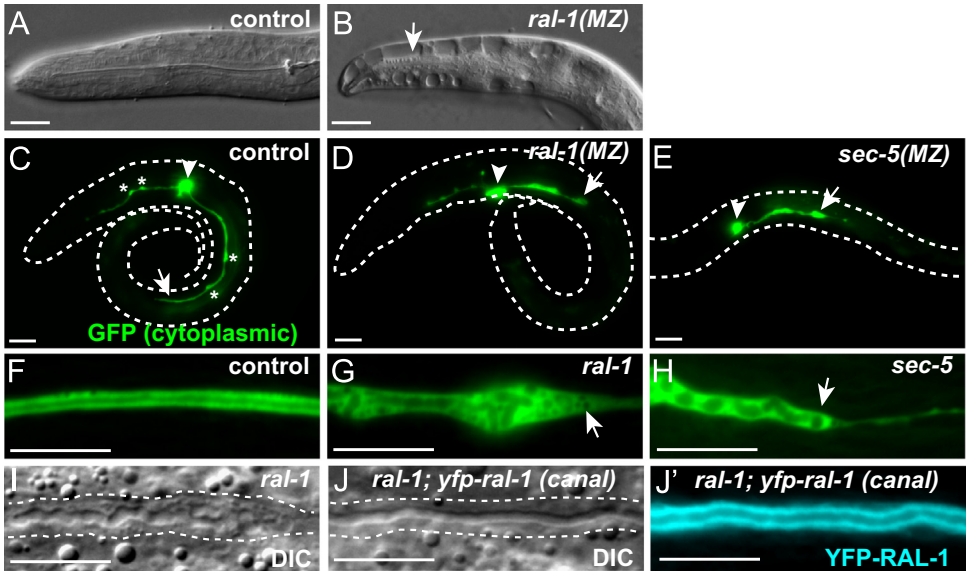

Fig. 2. *ral-1* and the exocyst are required for osmoregulation and excretory canal lumen extension. (A and B) Anterior end of control (A) and *ral-1*(*MZ*) (B) L1 larvae placed in water; arrow indicates fluid-filled cavity. (C–E) Newly hatched L1 larvae (body outlined) expressing cytoplasmic GFP in the excretory canal cell. Arrowhead points to canal cell body, arrow indicates posterior extent of canal outgrowth, and asterisks in (C) highlight periodic cytoplasmic 'pearls.' (F–H) Segment of posterior excretory canal in L4 larvae of indicated genotypes expressing cytoplasmic GFP; mutant canals in (G) and (H) terminate prematurely (arrow). (I–J′) *ral-1* mutant siblings lacking (I) or expressing (J and J′) canal-specific *Ppgp-12::yfp-ral-1* transgene. Dashed lines in (I) and (J) outline the canal, which is discontinuous in *ral-1* mutant (I) and smooth in rescued (J) canals; transgene expression in the rescued canal is shown in (J′). Scale bars are 10 μm.

numerous vesicular structures followed by a thin cytoplasmic extension (Fig. 2G and H), which in some animals extended well beyond the truncated lumen (Fig. S4A). The lumenized portion of excretory canals in *ral-1* and *sec-5* mutants often displayed abnormalities including irregular shape, variable width and septa (Fig. 2G–I). We tested whether *ral-1* function in the canal was sufficient to rescue lumenogenesis phenotypes by expressing *yfp-ral-1* from the *pgp-12* promoter. *ral-1*; *Ppgp-12::yfp-ral-1* animals formed normal, lumenized, and continuous canals [95%, $n=37$ in *ral-1*; *Ppgp-12::yfp-ral-1* versus 5%, $n=21$ in *ral-1* mutants alone, Chi-squared ($p<0.0001$)] (Fig. 2I–J′). We conclude that *ral-1* and the exocyst are required in the excretory cell for intracellular lumenization, but are dispensable for initial canal outgrowth.

Subcellular localization of RAL-1, the exocyst and PAR proteins within the excretory cell

In order to better understand RAL-1 and exocyst function during canal lumen formation, we examined their subcellular localization within the excretory cell. We first compared the distributions of YFP-RAL-1 and SEC-8-mCherry with each other, then with known markers of canal structures. Examined by immunoelectron microscopy, the intermediate filament protein IFB-1 localizes to the lumenal scaffold, while V-type ATPase subunit VHA-5 is found on canalicular vesicles (Kolotuev et al., 2013). YFP-RAL-1 had a broader distribution along the canal than SEC-8-mCherry (Fig. 3B–B″) but did not fill the width of the cell (Fig. S5). SEC-8-mCherry showed a similar distribution to IFB-1-GFP but not VHA-5-mCherry (Fig. 3C–C″, and E–E″), while YFP-RAL-1 localized similarly to VHA-5-mCherry (Fig. 3D–D″). To determine where PAR proteins are found within the excretory cell, we compared the distributions of PAR-3-GFP and SEC-8-mCherry. Similar to SEC-8-mCherry, PAR-3-GFP was lumenally restricted and punctate (Fig. 3F–F″). We conclude that the exocyst and PAR proteins are likely present at the lumenal surface, while RAL-1 is also likely found on canalicular vesicles.

ral-1 and sec-5 are required for osmotic shock recovery

Given the localization of the exocyst to the lumenal scaffold and YFP-RAL-1 to canalicular vesicles, we hypothesized that exocyst activity was required for the formation or fusion of lumenal canalicular vesicles. Recovery from hyperosmotic shock triggers the fusion of additional canalicular vesicles with the lumen, increasing its surface area and promoting water and ion flux (Khan et al., 2013; Kolotuev et al., 2013). The additional vesicles are thought to arise from cytoplasmic ER-rich swellings named 'pearls', which form transiently along the canal in response to an increased salt load but resolve after worms return to isotonic conditions (Kolotuev et al., 2013; Hahn-Windgassen and Van Gilst, 2009). Pearls are thought to coincide with active areas of canal membrane growth, and also occur during normal canal outgrowth in L1 larvae (see Fig. 2C). If the exocyst were required for the formation or lumenal fusion of canalicular vesicles, we reasoned that pearls induced by osmotic shock would persist in mutant larvae. Following osmotic shock, pearls induced in wild-type L4 larvae disappeared in 94% of animals within an hour after return to isotonic conditions (Fig. 4A–C, and G). By contrast, pearls disappeared in only 20% of *ral-1* and 36% of *sec-5* mutants within the same period (Fig. 4D–G), but had fully resolved by the following day (data not shown). Given the role of membrane expansion in pearl recovery from hyperosmotic shock, these findings are consistent with a role for RAL-1 and the exocyst in the production and/or fusion of canalicular vesicles at the lumenal surface.

ral-1 promotes apical fusion of canalicular vesicles

To visualize canalicular vesicles directly, we examined 200 nm thick sections of wild-type and *ral-1* excretory canals using electron tomography. We chose to examine *ral-1* zygotic mutants so that the architecture of the excretory canal was not severely abnormal, as in *ral-1*(*MZ*) mutants. Wild-type canals contained a single apical lumen and surrounding canalicular vesicles that occupied the majority of the canal cytoplasm (Fig. 5A). Canalicular

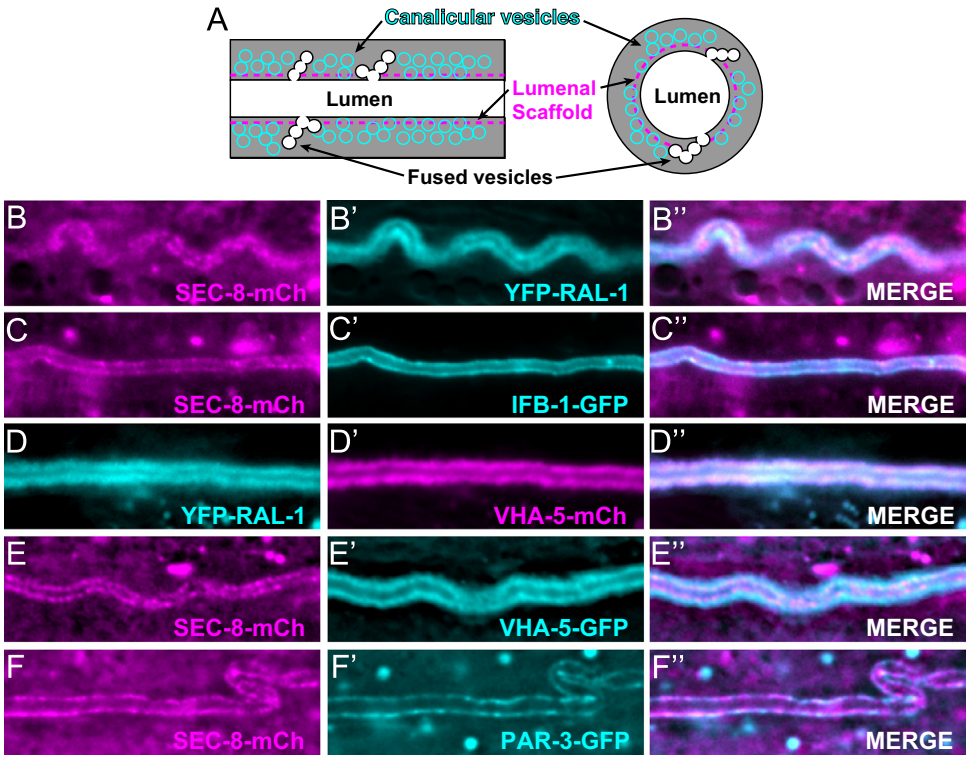

Fig. 3. Subcellular localization of RAL-1, the exocyst, and PAR proteins within the excretory canal. (A) Excretory canal schematic shown in lateral (left) and transverse (right) sections. (B–F″) Live images of excretory canals in L4 larvae co-expressing the indicated transgenes. Scale bar is 10 μm, and scale is equivalent in all images.

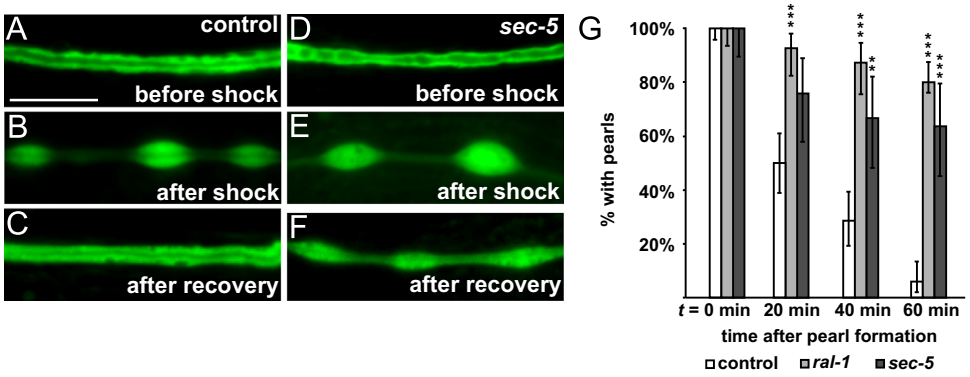

Fig. 4. *ral-1* and *sec-5* are required for prompt recovery from hyperosmotic shock. (A–C) Control larvae expressing canal-specific GFP before shock (A), 20 min after shock (B) and after one-hour recovery (C). (D–F) *sec-5* mutant expressing canal-specific GFP; pearls remain after the one-hour recovery. (G) Percentage of control ($n=84$), *ral-1* ($n=55$) and *sec-5* ($n=33$) mutants with cytoplasmic pearls following recovery from hyperosmotic shock; time zero corresponds to the first appearance of pearls following shock. Error bars represent the 95% confidence interval. $^{**}p < 0.001$, $^{***}p < 0.0001$, Chi-squared test of mutants *versus* control. Scale bars are 10 μm, and scale is equivalent in all panels.

vesicles were present as isolated vesicles, interconnected vesicles, and vesicles connected to the lumenal or basal surface by a pore or thin membrane (Fig. 5A′, C, and E), similar to previous observations (Kolotuev et al., 2013). Canals in *ral-1* mutants showed several prominent differences with wild type (Fig. 5B, D, and E, and Videos S1 and S2). First, we observed that *ral-1* mutant canals had a variable lumen diameter (see Fig. 2G and I) with significantly fewer vesicles along the canal than did wild type. A larger lumen diameter in *ral-1* canals could reflect dysfunction of the canal itself, as other mutants affecting excretory canal function can develop canal cysts (Buechner et al., 1999). Second, no canalicular vesicles were connected to the lumen, in contrast to the 23% of wild-type vesicles that were connected lumenally. Finally, a substantial number of vesicles in *ral-1* mutants were connected to the basal surface (22%) while basally connected vesicles were rare in wild type (1%). We conclude that *ral-1* is required for canalicular vesicles to fuse with the lumenal surface, and to prevent vesicles from associating with the basal surface. The decrease in canalicular vesicle number in *ral-1* mutants may indicate the presence of positive feedback between vesicle fusion and biogenesis, providing the cell with a mechanism to govern the number of canalicular vesicles needed for osmoregulation. Alternatively, *ral-1* may have an additional role in canalicular vesicle formation.

Supplementary material related to this article can be found online at http://dx.doi.org/10.1016/j.ydbio.2014.07.019.

To determine if increasing exocyst activity causes an increase in lumenogenesis, we over-expressed YFP-RAL-1 specifically in the excretory cell. *Pgp-12::yfp-ral-1* over-expression caused a dramatic expansion of the canal lumen, which accumulated numerous cysts connected to the lumen (Fig. 5F). Cyst formation was reduced following partial depletion of SEC-8, indicating that RAL-1 regulates lumen expansion through the exocyst [11% with cysts in

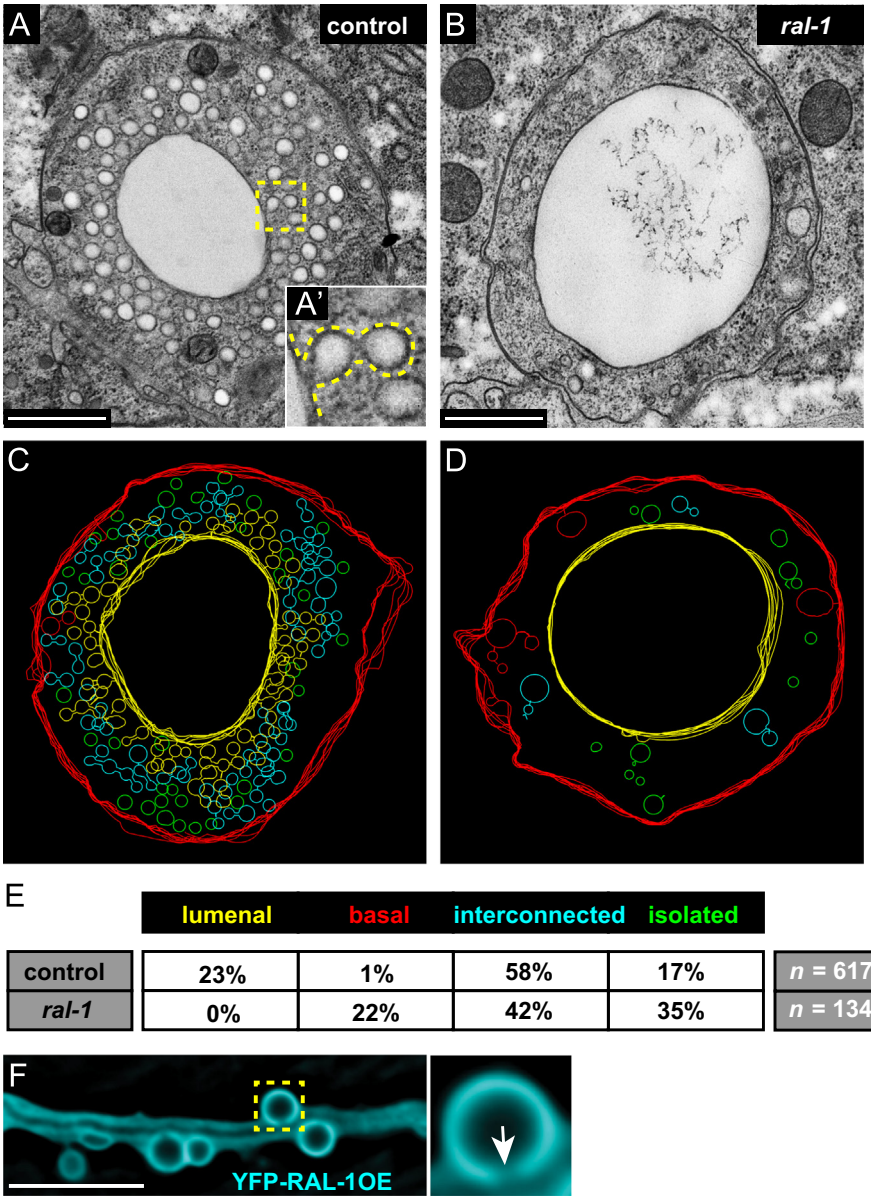

Fig. 5. *ral-1* is needed for vesicle fusion with the canal lumen. (A and A′) Representative transverse transmission electron microscopy (TEM) thin sections of the excretory canal in wild type (A) and *ral-1* mutants (B); sections were taken from the posterior canal between the pharynx and distal gonad. (A′) A higher magnification view of the boxed region in (A); interconnected vesicles fused to the lumen are outlined by a dotted line. Scale bars in (A) and (B) are 500 nm. (C and D) Tracings from 200 nm thick section TEM tomograms (see Videos S1 and S2 for raw data Z-stacks) from regions immediately distal to the sections displayed in panels (A) and (B). Each vesicle was outlined at its maximum diameter. Vesicles are classified as connected to the lumen (yellow), basal surface (red), interconnected (cyan), or isolated (green). (E) Summary of vesicle tracings from control (4 sections) and mutant (4 sections) tomograms; *n* refers to total number of vesicles from all sections combined. (F) L4 larval worm over-expressing YFP-RAL-1 specifically in the excretory canal. The magnified boxed region shows a cyst connected to the canal lumen (arrow). Scale bar is 10 μm.

sec-8 RNAi ($n=127$) *versus* 35% in control ($n=166$), Chi-squared ($p<0.0001$)]. Thus, while inactivation of the exocyst through *ral-1* depletion prevents canalicular vesicle fusion and lumen extension, over-activation of the exocyst through *ral-1* overexpression causes the lumen to expand.

PAR proteins function upstream to induce exocyst asymmetry in early embryonic cells

We hypothesized that PAR proteins polarize the exocyst and therefore promote vesicle fusion specifically at the lumenal surface. Addressing the role of PAR proteins in the excretory canal, which undergoes morphogenesis during late embryogenesis and larval stages, is complicated by the essential earlier requirements for these proteins during zygote polarization and epithelial cell formation (Totong et al., 2007; Achilleos et al., 2010). To circumvent these earlier requirements, we used a temperature-sensitive, partial loss-of-function allele of *pkc-3* to acutely reduce PKC-3 function during excretory canal morphogenesis in larval worms (Fievet et al., 2012). Excretory canals in *pkc-3*ts mutants contained septations (51%, $n=35$; Fig. 6A and B′), and in some cases terminated abruptly (11%, $n=35$) when compared to control larvae grown at the same temperature ($n=22$). Similar phenotypes were present in worms *trans*-heterozygous for *pkc-3*ts and a null allele of *pkc-3* (10/12 displayed septations), indicating that they are specific to reduction in *pkc-3* activity. Notably, the canal phenotypes of *pkc-3*ts mutants are similar to but less penetrant than those of *sec-5* and *ral-1* mutants (see Fig. 2G–I), consistent with a reduction but not elimination of *pkc-3* activity.

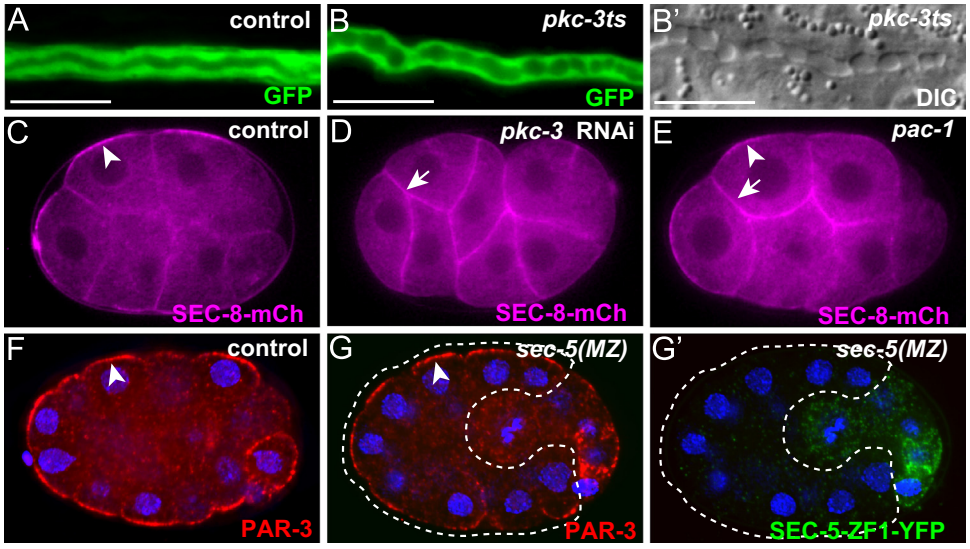

Fig. 6. PAR proteins in canal morphogenesis and exocyst polarity. (A–B′) Wild-type (A) and *pkc-3*ts mutant (B and B′) excretory canals from L4 larvae expressing GFP in the excretory canal and raised at 25 °C after late embryogenesis; DIC image in (B′) shows discontinuities of canal in B (compare to wild type in Fig. S1D and to similar *ral-1* mutant in Fig. 2I). Scale bars are 10 μm. (C and D) 8-Cell embryos from hermaphrodites expressing SEC-8-mCherry and fed with control bacteria containing empty vector (C) (n=66/66 polarized), or bacteria expressing *pkc-3* dsRNA (n=19/20 not polarized). (E) *pac-1* mutant 8-cell embryo expressing SEC-8-mCherry (n=16/16 not polarized). Arrowheads, SEC-8-mCherry at contact-free surfaces; arrows, SEC-8-mCherry at contacted surfaces. (F–G′) 26- to 28-cell stage control (n=24/24 polarized) (F) and mutant (n=13/13 polarized) (G and G′) embryos immunostained for indicated proteins. Dotted region in (G) and (G′) outlines mutant cells depleted of maternally provided SEC-5-ZF1-YFP protein. Arrowheads, PAR-3 enriched at contact-free surfaces.

To determine the hierarchy between PAR proteins and the exocyst, we examined their relationship in early embryonic cells, where PAR proteins, RAL-1 and the exocyst complex displayed asymmetries similar to those seen in the excretory canal, and where PAR protein function could be removed completely. To test whether PAR proteins are essential for exocyst asymmetry, we knocked down PAR-3, PAR-6 or PKC-3 using RNAi and examined the localization of SEC-8-mCherry. Following PAR knockdown, SEC-8-mCherry remained associated with the plasma membrane but its asymmetry was lost (Figs. 6C and D, and S6A and B). SEC-8-mCherry asymmetry was also lost in embryos depleted acutely of PAR-3 in early embryonic cells (Nance et al., 2003), suggesting a direct requirement for PAR proteins in exocyst asymmetry at this stage (Fig. S5C). In *pac-1* mutant early embryos, in which PAR-3, PAR-6, and PKC-3 are present but remain symmetric at the cell membrane, SEC-8-mCherry also remained symmetric (Fig. 6E) (Anderson et al., 2008). We conclude that PAR proteins must be present and asymmetric in order to induce exocyst asymmetry.

To determine if the exocyst functions downstream of PAR proteins or in parallel, we analyzed PAR protein localization in *ral-1*(*MZ*) and *sec-5*(*MZ*) early embryos. Similar to control embryos, PAR-3, PAR-6 and PKC-3 remained asymmetrically localized (Figs. 6F–G′ and S6D–H′). To determine the contribution of active RAL-1 to exocyst membrane localization, we over-expressed constitutively active RAL-1 (RAL-1CA) (Hinoi et al., 1996; Frische et al., 2007) in early embryos expressing SEC-8-mCherry. Cells expressing GFP-RAL-1CA uniformly recruited SEC-8-mCherry to all cell surfaces (Fig. 7A–B′) but had no effect on PAR protein asymmetry (Fig. 7C–D′). Therefore, RAL-1 is necessary (see Fig. S2) and active RAL-1 is sufficient to recruit the exocyst to the membrane, while PAR proteins are required to concentrate membrane-localized exocyst to a discrete cortical domain. We conclude that the exocyst functions downstream of RAL-1 and the PAR proteins.

Discussion

Our findings reveal a molecular pathway, centered on the vesicle-tethering exocyst complex, which promotes lumenogenesis within a seamless intracellular tube. Previously, it had been shown that seamless lumen formation and expansion within the excretory cell result from intracellular vesicle fusion at the lumenal membrane (Kolotuev et al., 2013; Khan et al., 2013). We have shown that the exocyst and its activator RAL-1 are essential for excretory cell lumen outgrowth, and that compromising exocyst activity (through RAL-1 depletion) prevents canalicular vesicle fusions with the lumen. Based on previous studies and our observations, we propose that RAL-1 and the exocyst promote lumenogenesis by directing lumenal vesicle fusion events. Consistent with such a role, we observed that loss of exocyst function resulted in delayed pearl recovery from hyperosmotic stress, which normally causes increased vesicle fusion events with the canal lumen (Kolotuev et al., 2013). In addition, increasing exocyst activity (through overexpression of RAL-1) resulted in a dramatic expansion of the excretory cell lumen. Controlling the activity of RAL-1 may therefore provide a mechanism to regulate the timing and rate of membrane addition during lumenogenesis.

Using polarized early embryonic cells, we have defined the relative contributions of RAL-1 and PAR proteins to exocyst localization and function. Several observations indicate that active RAL-1 recruits the exocyst to the membrane. First, removing RAL-1 caused exocyst components to become cytoplasmic. Second, expressing constitutively active RAL-1 recruited core exocyst components to ectopic membrane domains. Finally, the larval arrest phenotype of *ral-1*(*MZ*) mutants was remarkably similar to that displayed by *sec-5*(*MZ*) and *sec-8*(*MZ*) mutants, suggesting that exocyst regulation is the primary function for RAL-1 in *C. elegans*. We define a distinct function for PAR proteins in regulating exocyst asymmetry: removing PAR function by depleting PAR-3, PAR-6, or PKC-3, or by preventing polarized PAR localization *via pac-1* mutation, caused a loss of exocyst asymmetry without preventing membrane association. Thus, while RAL-1 promotes exocyst membrane recruitment, PAR proteins spatially restrict the exocyst to a membrane subdomain. Although we defined these relationships in experimentally accessible early embryonic cells, the analogous localization pattern of RAL-1, PAR proteins, and the exocyst within the excretory cell suggests that a similar relationship holds true in this cell as well. Testing this hypothesis is

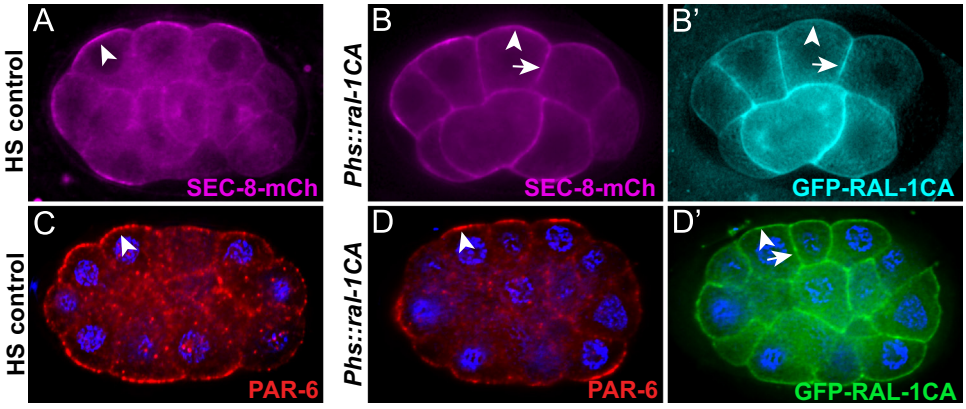

Fig. 7. Effect of RAL-1CA on the exocyst and PAR proteins. (A–B′) Heat-shock (HS) control embryo (A) or sibling embryos expressing heat-shock driven GFP-RAL-1CA (B and B′); all embryos express SEC-8-mCherry, which is enriched at contact-free surfaces (arrowheads) in control embryos ($n=50/50$ polarized) and recruited additionally to contacted surfaces (arrows) in embryos expressing RAL-1CA ($n=24/26$ ectopically recruited). (C–D′) HS control embryo immunostained for PAR-6 ($n=11/11$ polarized) (C), and sibling embryo expressing heat-shock driven GFP-RAL-1CA ($n=12/12$ polarized) (D and D′) co-immunostained for PAR-6 and GFP-RAL-1CA. Arrowheads show PAR-6 enrichment at contact-free surfaces; arrow indicates contacted surfaces.

complicated by the earlier essential function of PAR proteins and by maternal PAR protein contribution, and will require the development of new genetic tools to acutely remove PAR function at later developmental stages. Notably, a recent synthetic lethal RNAi screen identified genetic interactions between *pkc-3* and the exocyst, consistent with PAR proteins and the exocyst functioning together in multiple contexts during *C. elegans* development (Jiu et al., 2014).

The functional relationship between PAR proteins and the exocyst has been difficult to address in other systems. For example, knockdown experiments in MDCK cysts revealed that PAR proteins and the exocyst are mutually required for one another's asymmetric localization to the site of lumen formation (Bryant et al., 2010); it is not clear if this reflects true interdependency in PAR and exocyst localization, or whether removing PAR or exocyst function prevents the formation of a membrane domain or structure where the two protein complexes normally localize. Evidence from neuronal cell culture studies suggests that RalA may facilitate a direct interaction between Par6 and exocyst component Exo84 (Das et al., 2014). In *Drosophila* terminal tracheal cells, activity of the PAR protein aPKC is required for membrane enrichment of the exocyst component SEC-8 (Jones et al., 2014), although it is not known in this system whether the exocyst is similarly required for PAR protein localization. Using *C. elegans* early embryos, where PAR and exocyst function can be rapidly and acutely removed, we have shown that the exocyst clearly functions downstream of PAR proteins. PAR protein localization was unaffected by *ral-1* or *sec-5* mutation, and these mutants did not show the dramatic polarity phenotypes evident in *par* mutants.

How PAR proteins control exocyst localization remains unknown. One possibility is that PAR proteins physically bind the complex, enriching membrane-bound exocyst proteins within a distinct cortical domain. In support of this model, physical interactions have been observed between PAR proteins and several different exocyst complex members (see Introduction). Alternatively, given that constitutively active RAL-1 ectopically recruits the exocyst to sites lacking PAR proteins in early embryos, it is possible that PAR proteins asymmetrically enrich a Ral-activating protein, such as a guanine-nucleotide exchange factor (GEF), that locally activates RAL-1. For instance, PAR-3 recruits the Rac GEF TIAM1 to dendritic spines in neurons, and to tight junctions in epithelial cells, to spatially restrict Rac activation (Mertens et al., 2005; Chen and Macara, 2005; Zhang and Macara, 2006). In this way, PAR proteins would spatially restrict both exocyst membrane recruitment and asymmetry.

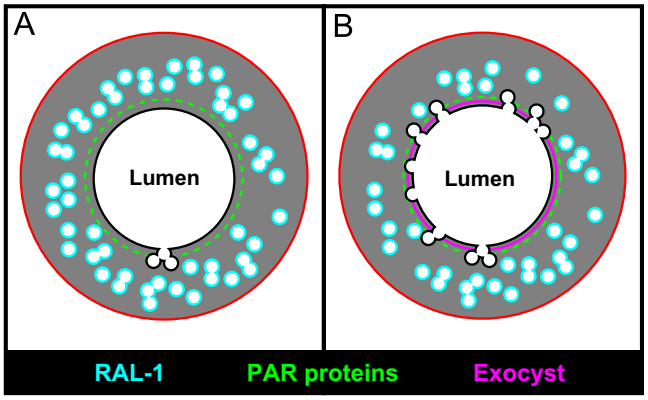

Fig. 8. Model for excretory canal lumen formation. (A) Schematic of the excretory canal shown in transverse section, with the PAR proteins (green) and RAL-1 (cyan) present at distinct but overlapping domains. (B) At regions containing both PAR proteins and active RAL-1, the exocyst (magenta) is recruited and triggers the docking and fusion of canalicular vesicles with the lumenal surface, leading to canal expansion and increased exchange of water and salt.

Based on these findings, we propose that lumen extension in the excretory cell occurs when the exocyst targets canalicular vesicles to dock at the growing lumenal surface, where RAL-1 and PAR proteins overlap (Fig. 8). How do PAR proteins associate specifically along the lumenal membrane? One possibility is that an asymmetric PAR membrane domain, established in the excretory cell body, invades the cytoplasm to produce the canal lumen. For instance, lumenal membrane invasion occurs within the terminal cells of the *Drosophila* trachea (Gervais and Casanova, 2010), and the *Ciona* notochord (Denker et al., 2013). Following this initial polarization event, exocyst-mediated vesicle fusion would then function to extend and expand the growing lumenal membrane. This hypothesis is supported by the observation that the nascent excretory canal lumen appears to expand from its junction with the adjacent duct cell (Mancuso et al., 2012).

The mechanisms we have identified are likely to work in concert with the ezrin–radixin–moesin protein ERM-1, which localizes to the excretory canal lumenal scaffold and is essential for linear canal growth and structural maintenance (Göbel et al., 2004). Loss of ERM-1 results in short, cystic canals that fail to elongate (Khan et al., 2013). ERM-1 interacts with aquaporin AQP-8,

which is present on canalicular vesicles, and is thought to help recruit AQP-8 to the lumenal surface. In turn, AQP-8 is thought to promote lumen expansion through water flux (Khan et al., 2013). Our findings show that RAL-1 and the exocyst are essential for canalicular fusion events, and are consistent with this model for ERM-1 function. However, *aqp-8*(*MZ*) null mutants are viable and form canals, in contrast to *ral-1*(*MZ*) and *sec-5*(*MZ*) mutants, indicating that ERM-1 recruitment of AQP-8 contributes to but is not essential for lumenogenesis.

Given the broad requirement for targeted vesicle fusion events in the lumenogenesis of seamless tubes, our findings suggest a mechanism for lumen formation that could operate in diverse cell types, including vertebrate vascular endothelial cells. Consistent with a conserved *in vivo* role for PAR proteins and the exocyst in seamless tube formation, *par-6*, *aPKC*, and exocyst components are required for intracellular lumenogenesis in *Drosophila* terminal tracheal cells (Jones and Metzstein, 2011; Jones et al., 2014). Together with findings in *Drosophila* tracheal cells, MDCK cysts (Bryant et al., 2010), and zebrafish intestinal cells (where *aPKCλ* is required for lumenogenesis) (Horne-Badovinac et al., 2001), our results suggest that intracellular and multicellular tubes, despite their fundamental differences in topology and organization, may form using common molecular mechanisms.

Materials and methods

Homolog identification

C. elegans Ral and exocyst homologs were determined by basic local alignment search tool (BLAST) search of the murine and *Drosophila* exocyst proteins against the *C. elegans* proteins (Wormbase release WS238). A single homolog was identified in the *C. elegans* genome for each gene. Reciprocal BLAST of *C. elegans* exocyst proteins against murine and *Drosophila* databases likewise identified highest scores for the respective homolog.

Strains

Strains used in this study are listed in Table S4. *sec-8*(*ok2187*) is an uncharacterized deletion allele isolated by the *C. elegans* Gene Knockout Consortium obtained from the *Caenorhabditis* Genetics Center (CGC, University of Minnesota), and was outcrossed four times. The *ok2187* deletion was verified using primers flanking the deletion (5′-cggctcaattcgactctgcc-3′ and 5′-cctttccaagtgctactacttctgg-3′) and internal primers to confirm loss of the deleted sequence (5′-gacgcgatatatcatcatctgcagtc-3′ and 5′-gagaacttgcttctcgtattgaaggag-3′). *ral-1*(*tm5205*) is an uncharacterized deletion allele isolated by the National Bioresource Project (kindly provided by Shohei Mitani) and was outcrossed five times. The *tm5205* deletion was verified with flanking primers (5′-ggcagaaatccaggaaaaagtgagg-3′ and 5′-gctttctgacgtaaaatacccaaaactcg-3′) and internal primers (5′-gtcgatttcccccgggttttc-3′ and 5′-cgacgtttttagagtctttgcatgcaaatttg-3′). The mutant *sec-5*(*pk2358*) was previously described (Frische et al., 2007) and was a kind gift from Fried Zwartkrius; we outcrossed the mutant three additional times. *pkc-3*(*ne4250*) was previously described (Fievet et al., 2012) and was a kind gift from Craig Mello; we outcrossed the mutant six times. All additional strains and mutants have been previously described, among which some were provided by the CGC.

Transgene construction

P*sec-8::sec-8-mCherry*, P*sec-8::sec-8-zf1-mCherry*, P*sec-5::sec-5-zf1-yfp*, P*ral-1::yfp-ral-1*, P*ral-1::zf1-yfp-ral-1*, and P*pgp-12::mCherry* were created by Gibson end-joining (Gibson et al., 2009). Fragments of genomic DNA or tags (see Table S5 for additional oligonucleotide information) were recombined into vector pJN566, which is a derivative of MosSCI vector pCFJ150 (Frøkjær-Jensen et al., 2008) modified to include a *Pme*I restriction site adjacent the *unc-119* coding region (using primers 5′-*Pme*I-ggcctagttctagacattctc-3′ and 5′-*Pme*I-cactggccgtcgttttacac-3′). Prior to Gibson end-joining, pJN566 was linearized by digestion with *Pme*I. PCR fragments to be assembled contained 40 bp homology arms with adjacent fragments, or with vector sequences flanking the *Pme*I site.

P*pgp-12::yfp-ral-1*, P*pgp-12::vha-5-gfp* and P*pgp-12::vha-5-mCherry* were generated by Gibson end-joining using vector pPD95.75 (Fire lab vector kit).

P*sec-10::mCherry-sec-10* and P*sec-15::sec-15-yfp* were created by fosmid recombineering using *galK* selection and SW105 cells, as described by Tursun et al. (2009).

For P*sec-10::mCherry-sec-10*, the following homology arms were used to insert *mCherry* amplified from plasmid pBALU4 (Tursun et al., 2009):

5′-gtatattttatattcaaaagtggtttttcatgctttaggaacaaataattacag-3′, and
5′-cggttcctgttctagatcctgtacatatgtcacatattgtccaccactcat-3′.

unc-119 was inserted into the LoxP site of P*sec-10::mCherry-sec-10* fosmid using plasmid pLoxPunc119 and SW106 cells, as described by Zhang et al. (2008).

For P*sec-15::sec-15-yfp*, the following homology arms were used to insert *yfp* amplified from plasmid pBALU2 (Tursun et al., 2009):

5′-cgcaagaagcttctcgacacaattgtccgtcagttgaaactcctggaaatt-3′, and
5′-taatcataccacagtaaaaggcaacataagtaacattaatttaaaaaatca-3′.

P*sec-15::sec-15-yfp* fosmid was then subcloned by gap repair into linearized pCFJ151 vector (Frøkjær-Jensen et al., 2008) using the following homology arms:

5′-gttcaaaaaaatagagggataaatgtttagttgtgttctgaactggtacac-3′, and
5′-tactgagttgaataagtattgattcttctctaactgtccgtcattcataac-3′.

P*hsp-16.2::gfp-ral-1CA* was generated by Gateway cloning (Invitrogen). Endogenous *ral-1* cDNA was amplified then cloned into the Gateway entry vector pDONR221, and then modified by PCR to generate a plasmid carrying *ral-1G26V* (*ral-1CA*) (Frische et al., 2007). This plasmid was then used in a Gateway LR reaction with a destination vector carrying the *hsp-16.2* promoter driving GFP (Chan and Nance, 2013) and *ral-1CA* was inserted downstream of the GFP sequence.

par-3 RNAi is directed against an exon of *par-3* and was cloned into the RNAi feeding vector pPD129.36 (Timmons et al., 2001).

P*par-6::par-6-mCherry* (Chan and Nance, 2013) and P*par-3::par-3-gfp* (Achilleos et al., 2010) plasmids and strains respectively were described previously.

Worm transformation

P*sec-8::sec-8-mCherry*, P*sec-8::sec-8-zf1-mCherry*, P*sec-5::sec-5-yfp*, P*sec-5::sec-5-zf1-yfp*, P*ral-1::yfp-ral-1*, P*ral-1::zf1-yfp-ral-1*, and P*sec-10::mCherry-sec-10* were transformed into worms by microparticle bombardment as described by Praitis et al. (2001), with minor modifications. *unc-119(ed3)* mutant worms were bombarded with the above constructs, which all contain an *unc-119* rescue cassette in *cis*. Plasmids were mixed 1:1 with pMA122 (Frøkjær-Jensen et al., 2012), which carries a heat-shock inducible *peel-1* toxin. Transformed, non-Unc worms were propagated several generations, and then heat-shocked at 34 °C for 2 h to

induce expression of the toxin, selecting against worms inheriting multicopy transgenes (those containing pMA122). At least two independent lines were analyzed for each construct.

P*sec-8::sec-8-mCherry* and P*sec-15::sec-15-yfp* were integrated into chromosome II in single copy by MosSCI (Frøkjær-Jensen et al., 2008). WM186 worms (Shirayama et al., 2012) (which contain the *ttTi5605* Mos1 insertion on chromosome II, are *unc-119*(*ed3*), and are resistant to ivermectin) were injected with a DNA mixture including pTG96 (P*sur-5::sur-5-gfp-NLS*) (Yochem et al., 1998) (33 ng/μL), pJL44 (P*hsp16.48::MosTase*) (Frøkjær-Jensen et al., 2008) (33 ng/μL), pCCM416 (P*myo-2::avr-15*) (Shirayama et al., 2012) (33 ng/μL) and the construct of interest (1 ng/μL); the vector backbone additionally includes *unc-119*(+) and homology arms flanking the *ttTi5605* Mos1 site. Transmitting lines (non-Unc, SUR-5-GFP expressing) were heat-shocked for 2 h at 34 °C to induce germline transposase expression. After two subsequent generations, single-copy integrants were identified by the ability to grow on NGM plates containing ivermectin (25 ng/mL) and by lack of SUR-5-GFP expression.

P*pgp-12::yfp-ral-1*, P*hsp-16.2::gfp-ral-1CA*, P*pgp-12::vha-5-gfp*, P*pgp-12::vha-5-mCherry*, and P*pgp-12::mCherry* were injected directly into the worm germline together with plasmids carrying either dominant *rol-6*(*su1006*) or *sur-5-gfp* to generate extrachromosomal arrays (Mello et al., 1991).

Heat shock over-expression of fluorescent transgenes

Worms were heat shocked as described previously (Chan and Nance, 2013). Embryos carrying an extrachromosomal array containing heat shock promoter *hsp-16.2* driven transgenes were placed in a 34 °C incubator for one hour, and then recovered at room temperature for 30 min. Then, embryos were either mounted on agarose pads and imaged live, or fixed then immunostained.

Immunostaining

Embryos were placed onto poly-L-lysine coated slides, freeze-cracked and fixed in methanol and paraformaldehyde as previously described (Anderson et al., 2008). The following primary antibodies and dilutions were used: rabbit anti-GFP, 1:2000 (Abcam), chicken anti-GFP, 1:1000 (Aves), rabbit anti-PAR-6, 1:20,000 (Schonegg and Hyman, 2006), mouse anti-PAR-3, 1:10 (Nance et al., 2003), rat anti-PKC-3, 1:400 (Tabuse et al., 1998), and mouse anti-ERM-1, 1:50 (Developmental Hybridoma Studies Bank, University of Iowa). Fluorescently conjugated, species-specific, cross-adsorbed secondary antibodies were used to detect primary antibodies. Stained specimens were mounted in DABCO (Sigma) and imaged as described below.

Generation of maternal-zygotic mutants

Worms homozygous for *ral-1*, *sec-5*, or *sec-8* mutations, and heterozygous for the respective ZF1-tagged rescuing transgene, were allowed to self-fertilize. 25% of the F1 progeny do not inherit the ZF1-tagged rescuing transgene (which is also expressed zygotically) and are therefore maternal-zygotic (*MZ*) mutants (protein inherited maternally from the transgene degrades in early embryos because of the ZF1 tag). A subset of embryos and larvae displaying the *MZ* phenotype were scored to confirm absence of transgene expression. *sec-5(MZ)* mutants were also obtained by allowing *sec-5* homozygous mutants to self-fertilize and examining the resulting progeny.

RNAi

RNAi was performed using the feeding method (Timmons et al., 2001). For *par* RNAi, experiments were performed on HT115 bacteria carrying the empty vector pPD129.36, or derivatives carrying cDNA of *par-3* (four repetitions) (this study, see above), *par-6* (six repetitions) (Anderson et al., 2008) or *pkc-3* (Chan and Nance, 2013). L4 worms were placed on plates seeded for 12 h with bacterial cultures that had been grown for 9 h at 37 °C. Worms were left on plates for 24–48 h and phenotypes were scored in the next generation in embryos. Analysis of PAR-6-GFP expression and localization was performed in parallel as a positive control for sufficient RNAi knockdown. *zif-1* RNAi was performed as described by DeRenzo et al. (2003).

sec-8 RNAi clone was obtained from the Vidal cDNA RNAi library (clone ID Y106G6H.7). For RNAi dilution experiments, HT115 bacteria carrying the *sec-8* RNAi plasmid were diluted with cultures grown simultaneously and carrying empty vector (pPD129.36). OD_{600} was measured after 9 h in liquid culture (37 °C) and serial dilutions were performed using equivalent amounts of bacteria from empty vector and *sec-8* RNAi expressing bacteria. Strong RNAi (100% *sec-8* RNAi) resulted in larval arrest in F1 worms, similar to *sec-8(MZ)* animals. Diluted RNAi (25%) produced no larval lethality, but sufficiently suppressed the *yfp-ral-1* over-expression phenotype.

Microscopy and image processing

Differential interference contrast (DIC) using Nomarski optics and fluorescence images were collected using a Zeiss AxioImager, 63× 1.4 NA or 40× 1.3 NA objective, an Axiocam MRM camera and AxioVision software. In AxioVision software, all images were deconvolved with an identical algorithm. Images were cropped in ImageJ (NIH) and control and mutant images processed similarly using Photoshop (Adobe), with no γ adjustments. For all live imaging experiments, embryos and larvae were mounted onto pads made from 4% agarose in M9 or water at room temperature, except where noted. Immunostained embryos were mounted in DABCO (Sigma) mounting medium.

Hyperosmotic shock

The hyperosmotic shock protocol was performed as described with minor modifications (Kolotuev et al., 2013). L4 larval worms were transferred to NGM plates containing excess salt (500 mM NaCl) for 30 min. Worms were left on plates for 30 min and then transferred to standard NGM plates (50 mM NaCl). Within 20 min of return to NGM plates, pearl regions formed along the excretory canals in a subset of animals. Animals were scored for the persistence of pearls every 20 min on a Zeiss M2Bio fluorescence microscope. A small percentage of both *ral-1* and *sec-5* mutants on standard NGM plates had pearls along their canals prior to osmotic shock; only those lacking pearls were selected for the assay.

Electron microscopy

We collected L4 stage control and *ral-1* mutant worms, where maternal protein in *ral-1* mutants would be largely depleted. Sections were analyzed only in the anterior half of posterior canals, a region which by light microscopy appears largely normal in *ral-1* mutants (see Fig. 2). 10–15 Worms were placed into 100 μm deep planchette hats with yeast paste. Hats were coated with hexadecane, sealed in the planchette holder and high pressure freezing was performed using a Wohlwend Compact HPF-01 High Pressure Freezer. Frozen hats were immediately transferred into liquid nitrogen, then to tubes containing 2%

osmium tetroxide and 1% uranyl acetate in acetone at liquid nitrogen temperature. Samples in tubes were moved from liquid nitrogen into a Leica EM AFS2 freeze substitution unit and left at −90 °C for 96 h. Unit temperature was raised 5 °C/h to −60 °C, incubated for 12 h, raised to −30 °C for an additional 12 h, and finally raised to 0 °C for 4 h. Three one hour exchanges of pure acetone at 0 °C were used to remove osmium. Infiltration at room temperature began with a 1:1 mixture of acetone and Embed 812 (Electron Microscopy Sciences, Hatfield, PA) for 1 h, followed by 1:2 overnight. Samples were allowed to sit in pure epon for 4 h before embedding. Worms were flat embedded with aclar embedding film and polymerized at 60 °C. Serial semi-thin sections were cut (UC6 microtome; Leica Microsystems) at 0.5 μm and stained with 1% Toluidine Blue to evaluate the quality of preservation and find the area of interest. Thin sections (60 nm for morphology or 200 nm for tomography) were cut and stained with uranyl acetate and lead citrate by standard methods. Stained grids were examined under a Philips CM-12 electron microscope and photographed with a Gatan (4k × 2.7k) digital camera.

Collection and analysis of EM tomograms

For tomogram collection, samples were tilted between −70° and +70° at one-degree intervals and electron micrographs were recorded at 15,000–25,000-fold magnification with a CM200 microscope (FEI Corporation, Hillsboro, OR, USA) equipped with a 2k × 2k CCD camera (TVIPS, Gauting, Germany). Dual-axis tilt series were collected with a high-tilt tomography holder (Fischione, Export, PA, USA) and the serial EM program for automated data collection (Mastronarde, 2005). A second tilt series of the same area was collected after manually rotating the specimen support by 90°. Dual-axis tomographic data were reconstructed by IMOD (Kremer et al., 1996). For modeling, features of interest within the tomogram volumes were segmented manually using the software AMIRA (Mercury Computer Systems, San Diego, CA, USA).

Statistics

For hyperosmotic shock experiments, total worms assayed over several experimental repetitions are represented in Fig. 4G, and bars represent the 95% confidence interval of each percentage. The experiment was repeated six times for controls (all with $<10\%$ pearls at 60 min time point), five times for *ral-1* (all with $>50\%$ pearls at 60 min), and twice for *sec-5* (each with $>50\%$ pearls at 60 min). Statistical comparison was performed using a two-tailed Chi-squared test. For *yfp-ral-1* over-expression and suppression, experiments were repeated three times, and each individual repetition contained a sample size of $n>20$. Samples did not vary significantly within each individual group between trials (as determined by the Chi-squared test). Total *n* worms scored over the three trials were then grouped together and overall worms scored were compared between groups using a Chi-squared test.

Acknowledgments

We thank Jane Hubbard, Niels Ringstad and Diana Klompstra for critical reading of the manuscript, and Yuliya Zilberman for helpful discussions. We thank the NYULMC OCS Microscopy Core, especially Kristen Dancel and Chris Petzold, for their assistance with TEM. We thank the CGC, Eve Stringhsam, Fried Zwartkruis, Shohei Mitani, Christopher Trzepacz and Craig Mello for strains. S.A and J.N. designed the experiments and interpreted results. S.A. generated all strains and performed all experiments, except electron microscopy, which was performed by E.C. S.A. and J.N. wrote the manuscript. This work was funded by NIH Grants R01GM098492 and R01GM078341 to J.N. and NIH NRSA fellowship F30DK093197 to S.A.

Appendix A. Supporting information

Supplementary data associated with this article can be found in the online version at http://dx.doi.org/10.1016/j.ydbio.2014.07.019.

References

Achilleos, A., Wehman, A.M., Nance, J., 2010. PAR-3 mediates the initial clustering and apical localization of junction and polarity proteins during *C. elegans* intestinal epithelial cell polarization. Development 137, 1833–1842. http://dx.doi.org/10.1242/dev.047647.

Anderson, D.C., Gill, J.S., Cinalli, R.M., Nance, J., 2008. Polarization of the *C. elegans* embryo by RhoGAP-mediated exclusion of PAR-6 from cell contacts. Science 320, 1771–1774. http://dx.doi.org/10.1126/science.1156063.

Andrew, D.J., Ewald, A.J., 2010. Morphogenesis of epithelial tubes: insights into tube formation, elongation, and elaboration. Dev. Biol. 341, 34–55. http://dx.doi.org/10.1016/j.ydbio.2009.09.024.

Boyd, C., 2004. Vesicles carry most exocyst subunits to exocytic sites marked by the remaining two subunits, Sec3p and Exo70p. J. Cell Biol. 167, 889–901. http://dx.doi.org/10.1083/jcb.200408124.

Bryant, D.M., Datta, A., Rodríguez-Fraticelli, A.E., Peränen, J., Martín-Belmonte, F., Mostov, K.E., 2010. A molecular network for de novo generation of the apical surface and lumen. Nat. Cell Biol. 12, 1035–1045. http://dx.doi.org/10.1038/ncb2106.

Brymora, A., Valova, V.A., Larsen, M.R., Roufogalis, B.D., Robinson, P.J., 2001. The brain exocyst complex interacts with RalA in a GTP-dependent manner: identification of a novel mammalian Sec3 gene and a second Sec15 gene. J. Biol. Chem. 276 (32), 29792–29797. http://dx.doi.org/10.1074/jbc.C100320200.

Buechner, M., Hall, D.H., Bhatt, H., Hedgecock, E.M., 1999. Cystic canal mutants in *Caenorhabditis elegans* are defective in the apical membrane domain of the renal (excretory) cell. Dev. Biol. 214, 227–241. http://dx.doi.org/10.1006/dbio.1999.9398.

Chan, E., Nance, J., 2013. Mechanisms of CDC-42 activation during contact-induced cell polarization. J. Cell Sci. 126, 1692–1702. http://dx.doi.org/10.1242/jcs.124594.

Chen, X., Macara, I.G., 2005. Par-3 controls tight junction assembly through the Rac exchange factor Tiam1. Nat. Cell Biol. 7, 262–269. http://dx.doi.org/10.1038/ncb1226.

Das, A., Gajendra, S., Falenta, K., Oudin, M.J., Peschard, P., Feng, S., et al., 2014. RalA promotes a direct exocyst-Par6 interaction to regulate polarity in neuronal development. J. Cell Sci. 127, 686–699. http://dx.doi.org/10.1242/jcs.145037.

Davis, G.E., Camarillo, C.W., 1996. An *a2b1* integrin-dependent pinocytic mechanism involving intracellular vacuole formation and coalescence regulates capillary lumen and tube formation in three-dimensional collagen matrix. Exp. Cell Res. 224, 39–51. http://dx.doi.org/10.1006/excr.1996.0109.

DeRenzo, C., Reese, K.J., Seydoux, G., 2003. Exclusion of germ plasm proteins from somatic lineages by cullin-dependent degradation. Nature 424, 685–689. http://dx.doi.org/10.1038/nature01887.

Denker, E., Bocina, I., Jiang, D., 2013. Tubulogenesis in a simple cell cord requires the formation of bi-apical cells through two discrete Par domains. Development 140, 2985–2996. http://dx.doi.org/10.1242/dev.092387.

Fievet, B.T., Rodriguez, J., Naganathan, S., Lee, C., Zeiser, E., Ishidate, T., Shirayama, M., Grill, S.W., Ahringer, J., 2012. Systematic genetic interaction screens uncover cell polarity regulators and functional redundancy. Nat. Cell Biol. 15, 103–112. http://dx.doi.org/10.1038/ncb2639.

Frische, E.W., Pellis-van Berkel, W., van Haaften, G., Cuppen, E., Plasterk, R.H.A., Tijsterman, M., Bos, J.L., Zwartkruis, F.J.T., 2007. RAP-1 and the RAL-1/exocyst pathway coordinate hypodermal cell organization in *Caenorhabditis elegans*. EMBO J. 26, 5083–5092. http://dx.doi.org/10.1038/sj.emboj.7601922.

Frøkjær-Jensen, C., Wayne Davis, M., Jorgensen, E.M., 2008. Single-copy insertion of transgenes in *Caenorhabditis elegans*. Nat. Genet. 40, 1375–1383. http://dx.doi.org/10.1038/ng.248.

Frøkjær-Jensen, C., Davis, M.W., Ailion, M., Jorgensen, E.M., 2012. Improved Mos1-mediated transgenesis in *C. elegans*. Nat. Methods 9, 117–118. http://dx.doi.org/10.1038/nmeth.1865.

Gervais, L., Casanova, J., 2010. *In vivo* coupling of cell elongation and lumen formation in a single cell. Curr. Biol. 20, 359–366. http://dx.doi.org/10.1016/j.cub.2009.12.043.

Gibson, D.G., Young, L., Chuang, R.-Y., Venter, J.C., Hutchison, C.A., Smith, H.O., 2009. Enzymatic assembly of DNA molecules up to several hundred kilobases. Nat. Methods 6, 343–345. http://dx.doi.org/10.1038/nmeth.1318.

Göbel, V., Barrett, P.L., Hall, D.H., Fleming, J.T., 2004. Lumen morphogenesis in *C. elegans* requires the membrane-cytoskeleton linker *erm-1*. Dev. Cell 6, 865–873. http://dx.doi.org/10.1016/j.devcel.2004.05.018.

Hahn-Windgassen, A., Van Gilst, M.R., 2009. The *Caenorhabditis elegans* HNF4alpha Homolog, NHR-31, mediates excretory tube growth and function through

coordinate regulation of the vacuolar ATPase. PLoS Genet. 5, e1000553. http://dx.doi.org/10.1371/journal.pgen.1000553.
He, B., Guo, W., 2009. The exocyst complex in polarized exocytosis. Curr. Opin. Cell Biol. 21, 537–542. http://dx.doi.org/10.1016/j.ceb.2009.04.007.
Herwig, L., Blum, Y., Krudewig, A., Ellertsdottir, E., Lenard, A., Belting, H.-G., Affolter, M., 2011. Distinct cellular mechanisms of blood vessel fusion in the zebrafish embryo. Curr. Biol. 21, 1942–1948. http://dx.doi.org/10.1016/j.cub.2011.10.016.
Hinoi, T., Kishida, S., Koyama, S., Ikeda, M., Matsuura, Y., Kikuchi, A., 1996. Post-translational modifications of Ras and Ral are important for the action of Ral GDP dissociation stimulator. J. Biol. Chem. 271, 19710–19716.
Horne-Badovinac, S., Lin, D., Waldron, S., Schwarz, M., Mbamalu, G., Pawson, T., Jan, Y., Stainier, D.Y., Abdelilah-Seyfried, S., 2001. Positional cloning of *heart and soul* reveals multiple roles for PKC lambda in zebrafish organogenesis. Curr. Biol. 11, 1492–1502.
Iruela-Arispe, M.L., Davis, G.E., 2009. Cellular and molecular mechanisms of vascular lumen formation. Dev. Cell 16, 222–231. http://dx.doi.org/10.1016/j.devcel.2009.01.013.
Jiu, Y., Hasygar, K., Tang, L., Liu, Y., Holmberg, C.I., Bürglin, T.R., Hietakangas, V., Jäntti, J., 2014. *par-1*, atypical *pkc*, and PP2A/B55 *sur-6* are implicated in the regulation of exocyst-mediated membrane trafficking in *Caenorhabditis elegans*. Genes Genome Genet. 4, 173–183.
Johnston, D.S., Ahringer, J., 2010. Cell polarity in eggs and epithelia: parallels and diversity. Cell 141, 757–774. http://dx.doi.org/10.1016/j.cell.2010.05.011.
Jones, T.A., Metzstein, M.M., 2011. A novel function for the PAR complex in subcellular morphogenesis of tracheal terminal cells in *Drosophila melanogaster*. Genetics 189, 153–164. http://dx.doi.org/10.1534/genetics.111.130351.
Jones, T.A., Nikolova, L.S., Schjelderup, A., & Metzstein, M.M. (2014). Exocyst-mediated membrane trafficking is required for branch outgrowth in *Drosophila* tracheal terminal cells. Dev. Biol. 10.1016/j.ydbio.2014.02.021.
Khan, L.A., Zhang, H., Abraham, N., Sun, L., Fleming, J.T., Buechner, M., Hall, D.H., Göbel, V., 2013. Intracellular lumen extension requires ERM-1-dependent apical membrane expansion and AQP-8-mediated flux. Nat. Cell Biol. 15, 143–156. http://dx.doi.org/10.1038/ncb2656.
Kolotuev, I., Hyenne, V., Schwab, Y., Rodriguez, D., Labouesse, M., 2013. A pathway for unicellular tube extension depending on the lymphatic vessel determinant Prox1 and on osmoregulation. Nat. Cell Biol. 15, 157–168. http://dx.doi.org/10.1038/ncb2662.
Kremer, J.R., Mastronarde, D.N., McIntosh, J.R., 1996. Computer visualization of three-dimensional image data using IMOD. J. Struct. Biol. 116, 71–76. http://dx.doi.org/10.1006/jsbi.1996.0013.
Lalli, G., 2009. RalA and the exocyst complex influence neuronal polarity through PAR-3 and aPKC. J. Cell Sci. 122, 1499–1506. http://dx.doi.org/10.1242/jcs.044339.
Lipschutz, J.H., Guo, W., O'Brien, L.E., Nguyen, Y.H., Novick, P., Mostov, K.E., 2000. Exocyst is involved in cystogenesis and tubulogenesis and acts by modulating synthesis and delivery of basolateral plasma membrane and secretory proteins. Mol. Biol. Cell 11, 4259–4275.
Liu, J., Guo, W., 2012. The exocyst complex in exocytosis and cell migration. Protoplasma 249, 587–597. http://dx.doi.org/10.1007/s00709-011-0330-1.
Mancuso, V.P., Parry, J.M., Storer, L., Poggioli, C., Nguyen, K.C.Q., Hall, D.H., Sundaram, M.V., 2012. Extracellular leucine-rich repeat proteins are required to organize the apical extracellular matrix and maintain epithelial junction integrity in *C. elegans*. Development 139, 979–990. http://dx.doi.org/10.1242/dev.075135.
Mastronarde, D.N., 2005. Automated electron microscope tomography using robust prediction of specimen movements. J. Struct. Biol. 152, 36–51. http://dx.doi.org/10.1016/j.jsb.2005.07.007.
Mello, C.C., Kramer, J.M., Stinchcomb, D., Ambros, V., 1991. Efficient gene transfer in *C. elegans*: extrachromosomal maintenance and integration of transforming sequences. EMBO J. 10, 3959–3970.
Mertens, A.E.E., Rygiel, T.P., Olivo, C., van der Kammen, R., Collard, J.G., 2005. The Rac activator Tiam1 controls tight junction biogenesis in keratinocytes through binding to and activation of the Par polarity complex. J. Cell Biol. 170, 1029–-1037. http://dx.doi.org/10.1083/jcb.200502129.
Moskalenko, S., Tong, C., Rosse, C., Mirey, G., Formstecher, E., Daviet, L., Camonis, J., White, M.A., 2003. Ral GTPases regulate exocyst assembly through dual subunit interactions. J. Biol. Chem. 278, 51743–51748. http://dx.doi.org/10.1074/jbc.M308702200.
Moskalenko, S., Henry, D.O., Rosse, C., Mirey, G., Camonis, J.H., White, M.A., 2002. The exocyst is a Ral effector complex. Nature 4, 66–72. http://dx.doi.org/10.1038/ncb728.
Nance, J., Zallen, J.A., 2011. Elaborating polarity: PAR proteins and the cytoskeleton. Development 138, 799–809. http://dx.doi.org/10.1242/dev.053538.
Nance, J., Munro, E.M., Priess, J.R., 2003. *C. elegans* PAR-3 and PAR-6 are required for apicobasal asymmetries associated with cell adhesion and gastrulation. Development 130, 5339–5350. http://dx.doi.org/10.1242/dev.00735.
Nelson, F.K., Riddle, D.L., 1984. Functional study of the *Caenorhabditis elegans* secretory–excretory system using laser microsurgery. J. Exp. Zool. 231, 45–56. http://dx.doi.org/10.1002/jez.1402310107.
Nelson, F.K., Albert, P.S., Riddle, D.L., 1983. Fine structure of the *Caenorhabditis elegans* secretory–excretory system. J. Ultrastruct. Res. 82, 156–171.
Praitis, V., Casey, E., Collar, D., Austin, J., 2001. Creation of low-copy integrated transgenic lines in *Caenorhabditis elegans*. Genetics 157, 1217–1226.
Reese, K.J., Dunn, M.A., Waddle, J.A., Seydoux, G., 2000. Asymmetric segregation of PIE-1 in *C. elegans* is mediated by two complementary mechanisms that act through separate PIE-1 protein domains. Mol. Cell 6, 445–455.
Rosse, C., Formstecher, E., Boeckeler, K., Zhao, Y., Kremerskothen, J., White, M.D., Camonis, J.H., Parker, P.J., 2009. An aPKC-exocyst complex controls paxillin phosphorylation and migration through localised JNK1 activation. PLoS Biol. 7, e1000235. http://dx.doi.org/10.1371/journal.pbio.1000235.g007.
Schonegg, S., Hyman, A.A., 2006. CDC-42 and RHO-1 coordinate acto-myosin contractility and PAR protein localization during polarity establishment in *C. elegans* embryos. Development 133, 3507–3516. http://dx.doi.org/10.1242/dev.02527.
Schottenfeld-Roames, J., Ghabrial, A.S., 2012. Whacked and Rab35 polarize dynein–motor-complex-dependent seamless tube growth. Nat. Cell Biol. 14, 386–393. http://dx.doi.org/10.1038/ncb2454.
Shirayama, M., Seth, M., Lee, H.-C., Gu, W., Ishidate, T., Conte, D., Mello, C.C., 2012. piRNAs initiate an epigenetic memory of nonself RNA in the *C. elegans* germline. Cell 150, 65–77. http://dx.doi.org/10.1016/j.cell.2012.06.015.
Sugihara, K., Asano, S., Tanaka, K., Iwamatsu, A., Okawa, K., Ohta, Y., 2002. The exocyst complex binds the small GTPase RalA to mediate filopodia formation. Nat. Cell Biol. 4 (1), 73–78. http://dx.doi.org/10.1038/ncb720.
Tabuse, Y., Izumi, Y., Piano, F., Kemphues, K.J., Miwa, J., Ohno, S., 1998. Atypical protein kinase C cooperates with PAR-3 to establish embryonic polarity in *Caenorhabditis elegans*. Development 125, 3607–3614.
Timmons, L., Court, D.L., Fire, A., 2001. Ingestion of bacterially expressed dsRNAs can produce specific and potent genetic interference in *Caenorhabditis elegans*. Gene 263, 103–112.
Totong, R., Achilleos, A., Nance, J., 2007. PAR-6 is required for junction formation but not apicobasal polarization in *C. elegans* embryonic epithelial cells. Development 134, 1259–1268. http://dx.doi.org/10.1242/dev.02833.
Tursun, B., Cochella, L., Carrera, I., Hobert, O., 2009. A toolkit and robust pipeline for the generation of fosmid-based reporter genes in *C. elegans*. PLoS ONE 4, e4625. http://dx.doi.org/10.1371/journal.pone.0004625.
van Dam, E.M., Robinson, P.J., 2006. Ral: mediator of membrane trafficking. Int. J. Biochem. Cell Biol. 38, 1841–1847. http://dx.doi.org/10.1016/j.biocel.2006.04.006.
Yochem, J., Gu, T., Han, M., 1998. A new marker for mosaic analysis in *Caenorhabditis elegans* indicates a fusion between hyp6 and hyp7, two major components of the hypodermis. Genetics 149, 1323–1334.
Zhang, H., Macara, I.G., 2006. The polarity protein PAR-3 and TIAM1 cooperate in dendritic spine morphogenesis. Nat. Cell Biol. 8, 227–237. http://dx.doi.org/10.1038/ncb1368.
Zhang, Y., Nash, L., Fisher, A.L., 2008. A simplified, robust, and streamlined procedure for the production of *C. elegans* transgenes via recombineering. BMC Dev. Biol. 8, 119. http://dx.doi.org/10.1186/1471-213X-8-119.
Zhao, Z., Fang, L., Chen, N., Johnsen, R.C., Stein, L., Baillie, D.L., 2005. Distinct regulatory elements mediate similar expression patterns in the excretory cell of *Caenorhabditis elegans*. J. Biol. Chem. 280, 38787–38794. http://dx.doi.org/10.1074/jbc.M505701200.
Zuo, X., Fogelgren, B., Lipschutz, J.H., 2011. The small GTPase Cdc42 is necessary for primary ciliogenesis in renal tubular epithelial cells. J. Biol. Chem. 286, 22469–22477. http://dx.doi.org/10.1074/jbc.M111.238469.
Zuo, X., Guo, W., Lipschutz, J.H., 2009. The exocyst protein Sec10 is necessary for primary ciliogenesis and cystogenesis *in vitro*. Mol. Biol. Cell 20, 2522–2529. http://dx.doi.org/10.1091/mbc.E08-07-0772.